ACI STRUCTURAL JOURNAL TECHNICAL PAPER

Title no. 100-S18

Intrinsic Response Control of Moment-Resisting Frames Utilizing Advanced Composite Materials and Structural Elements

by Gregor Fischer and Victor C. Li

This paper reports on a research project aimed at investigating the response mechanism of a composite moment-resisting frame system with self-centering and energy dissipation capabilities. The suggested configuration of a particular composite beam and column members in a portal frame structure, serving as a simplified example of a moment-resisting frame system, can accommodate relatively large, inelastic deflections of the beam without formation of plastic hinges at the column bases. The combination of engineered cementitious composites (ECC) and fiber-reinforced polymers (FRP) reinforcement results in column elements with relatively high flexural strength and sufficient elastic deflection capacity to permit frame sway and prevent the formation of a collapse mechanism due to lateral loading. The load-deformation response is primarily influenced by an intrinsic transition mechanism of the relative flexural stiffness of beam and column members, triggered by the formation of plastic hinges in the beam. This concept is theoretically outlined and experimentally verified by tests using small-scale frame specimens under reversed cyclic loading conditions. Furthermore, the response of the tested specimens is analytically derived and compared with experimentally obtained data. The spectrum of responses obtained with this suggested configuration demonstrates the potential to design this configuration for a specific bilinear system behavior.

Keywords: composite; damage; moment; reinforcement; resistance; tolerance.

INTRODUCTION

The flexural load-deformation behavior of steel reinforced concrete members in terms of stiffness and strength is strongly influenced by the elastic limit of the reinforcing steel in tension. At yielding of the reinforcement and formation of a plastic hinge in an under-reinforced member, the flexural strength is essentially reached, while the flexural stiffness decays rapidly at further increasing inelastic deflections. Due to the relatively high modulus of elasticity of steel reinforcement (E_s = 210 GPa), the elastic flexural stiffness of a member with given geometry is also relatively large; however, the elastic strain capacity of the longitudinal steel reinforcement in tension (ε_{el} = 0.2%) results in very limited elastic deflection capacity of the steel-reinforced member.

In most structural applications of steel-reinforced concrete, a large flexural stiffness is desirable and required in order to limit member deflections under service load conditions for which the elastic deflection limit can be small and must not be exceeded. In seismic-resistant structures, however, inelastic deformations at particular locations of the structural system are intended to dissipate energy, thereby reducing the effects of seismic excitation on the structure. In particular, moment-resisting frames designed according to the strong column/weak beam concept are expected to undergo inelastic deformations by formation of plastic hinges in the beam members, while the columns remain elastic in order to maintain vertical load-carrying capacity and prevent possible collapse (Fig. 1(a)).

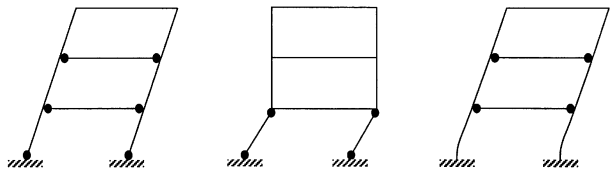

Fig. 1—Frame deformation modes.

Although the required flexural strength differential between beams and columns at joint locations enforces this ideal frame deformation mechanism and column members above the first story deform within their elastic limits, plastic hinges at the base of the first-story columns are necessary to initiate frame sway and inelastic deformations in the beam members (Paulay and Priestley 1992). The formation of plastic hinges at the column bases is inevitable and not immediately critical for the stability of the structure providing other plastic hinges form exclusively in beam members. There are disadvantages related to inelastic deformations at the column bases, however, with respect to detailing requirements, residual deformations, and rehabilitation needs. Expected plastic hinge regions must be properly detailed to provide confinement, shear resistance, and protection against buckling of longitudinal reinforcement. Residual deflections after experiencing inelastic deformations on the element and structural system level may, in addition, require extensive rehabilitation efforts. Furthermore, the possibility of exceeding the moment capacity of columns above the first floor or at the top of the first-story columns constitutes a potential failure mechanism (Fig. 1(b)).

Structural systems with self-centering capabilities after experiencing large, nonlinear deformations commonly use unbonded post-tensioned steel tendons in various types of construction, such as precast concrete (Priestley, Sritharan, and Conley 1999; El-Sheikh, Sause, and Pessiki 1999; Kurama, Pessiki, and Sause 1999) and steel structures (Ricles, Sause, and Garlock 2001). Although these high-strength steel tendons usually have a larger elastic strain limit compared to mild steel reinforcement, it is still necessary to distribute their elongation over an extended length to avoid yielding and,

ACI Structural Journal, V. 100, No. 2, March-April 2003.
MS No. 01-377 received November 14, 2001, and reviewed under Institute publication policies. Pertinent discussion will be published in the January-February 2004 *ACI Structural Journal* if received by September 1, 2003.

Gregor Fischer *is an assistant professor in the Department of Civil and Environmental Engineering at the University of Hawaii at Manoa. He received his PhD and MSE from the University of Michigan. His research interests include the design of fiber-reinforced cement composites and their structural applications.*

Victor C. Li *is a professor in the Department of Civil and Environmental Engineering at the University of Michigan. His research interests include micromechanics-based design of fiber-reinforced cementitious composites and integrated materials-structural design for performance enhancement, including repair and retrofit of infrastructures.*

consequently, unbonded reinforcement is required. Due to the absence of composite action between reinforcement and concrete in unbonded post-tensioned concrete members, however, the relatively large strain demand on concrete in compression at the (single) crack or interface location may impose limitations on the deformation and load-carrying capacity of the member.

In this paper, a moment-resisting frame configuration is investigated in which the formation of plastic hinges at the column bases of the first story is not required to initiate frame sway and subsequent formation of plastic hinges in the beam members (Fig. 1(c)). The use of fiber-reinforced polymer (FRP) reinforcement in combination with fiber-reinforced engineered cementitious composites (ECC) provides structural composite members with relatively large, elastic deflection capacity and flexural strength (Fischer and Li 2003). On the structural composite level, the deformation mechanism of these members is affected by the particular interaction of an elastic, fully bonded reinforcing material (FRP) combined with a ductile cementitious matrix (ECC) with strain hardening and multiple cracking behavior. These characteristic properties of ECC are required for the distribution of deformation along the flexural member to achieve a relatively large elastic deflection capacity, which constitutes the essential link between engineered material properties and structural composite deformation behavior. The design basis and mechanical properties of ECC are reviewed elsewhere (Li 1998). The elastic deflection capacity of FRP-reinforced ECC column members is expected to permit sufficient frame sway to initiate the formation of plastic hinges in the beam and use their inelastic deformation capacity for energy dissipation.

The use of FRP reinforcement in research projects and structural applications is often justified by its corrosion resistance (ACI Committee 440 1996). Investigations generally conclude that the flexural stiffness of FRP-reinforced concrete members is lower compared with those with an identical amount of steel reinforcement (ACI Committee 440 1996). Maximum deflections observed in FRP-reinforced concrete members, however, are small compared with the inelastic deflection capacity of steel-reinforced members. It has also been recognized that FRP-reinforced concrete members provide insufficient ductility due to the material properties of the longitudinal reinforcement (ACI Committee 440 1996). Attempts to overcome this deficiency include ductile compression failure of concrete by providing confinement reinforcement or using fiber-reinforced concrete (Naaman and Jeong 1995; Alsayed and Alhozaimy 1999), as well as hybrid FRP reinforcement with inherent ductility (Harris, Samboonsong, and Ko 1998). A large-scale experimental investigation was conducted on the structural performance of aramid FRP-reinforced concrete members exclusively used in a moment-resisting frame (Fukuyama et al. 1995). Structural elements with inelastic deformation capacity for energy dissipation were not provided. This study found small residual deflections after unloading as well as a stable hysteresis until crushing of concrete at 2% drift. Besides flexural cracking at the column bases, damage occurred by formation of splitting cracks along the longitudinal reinforcement in the beam followed by reinforcement rupture at 5% drift.

The portal frame structure presented in this paper consists of FRP-reinforced ECC column members and steel-reinforced ECC beams. This arrangement is expected to take advantage of the elastic deformation characteristics of the column members while dissipating energy by inelastic rotations in the beam plastic hinges. The substitution of concrete with ductile ECC in the FRP-reinforced columns, in particular, is necessary to achieve a relatively large elastic deflection capacity by distributing the flexural deformation over an extended portion of the member (Fischer and Li 2003). The damage-tolerant deformation behavior of ECC in tension also results in a stable hysteretic load-deformation response and prevents premature member failure. In addition, transverse reinforcement in the form of stirrups is not required throughout the entire structure due to the intrinsic shear resistance and confinement effect of the cementitious material (ECC) used in this study (Fischer and Li 2002).

The suggested frame system is expected to show a bilinear load-deformation response with considerable energy absorption and reduced residual displacements. The potential for auto-adaptive stiffness modification of the moment-resisting frame structure by selecting appropriate type and amount of reinforcement in beam and column members is investigated.

In the following, the anticipated deformation mechanism is conceptually outlined, experimentally verified, and contrasted to conventional steel-reinforced concrete configurations using small-scale specimens. Based on the conceptual outline, theoretical approaches to predict the load-deformation response of the suggested frame system are presented and compared with experimental results.

RESEARCH SIGNIFICANCE

In this paper, the load-deformation response of a composite frame system under reversed cyclic loading conditions is investigated and compared to a conventional frame configuration exclusively using steel reinforcement. The behavior of the suggested frame configuration is evaluated with respect to load-deformation response, specifically stiffness, energy dissipation, and residual displacements, as well as damage evolution and detailing requirements. Conclusions drawn from the research activities described in this paper may serve as a basis for an alternative approach to the design of seismic-resistant structures with improved performance in terms of dynamic response, residual displacement, damage tolerance, and rehabilitation requirements.

Frame response concept

The load-deformation response of the portal frame structure used in this study is affected by the respective flexural stiffness and length of the beam and column elements. The flexural stiffness of the individual elements varies depending on the degree of deflection as a result of successive flexural cracking and nonlinear compressive deformations in the cementitious matrix, as well as the tensile stress-strain behavior of the longitudinal reinforcement.

Yielding of steel reinforcement results in the formation of a plastic hinge in the flexural member, observed in the load-deformation response as a progressive reduction in flexural stiffness at a moment M_y and deflection Δy (Fig. 2). Beyond

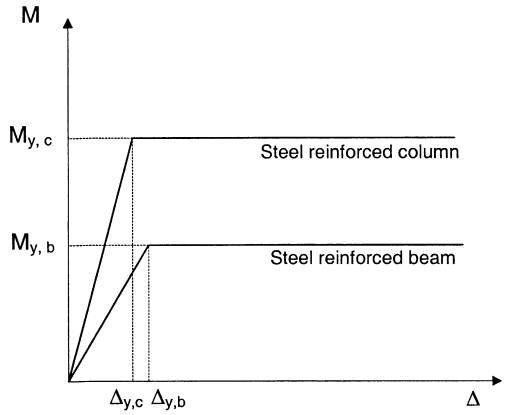

Fig. 2—Moment-deflection relationship of steel-reinforced members.

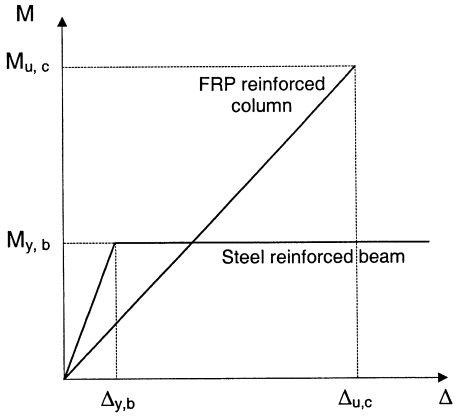

Fig. 4—Moment-deflection relationship of FRP-reinforced member and steel-reinforced member.

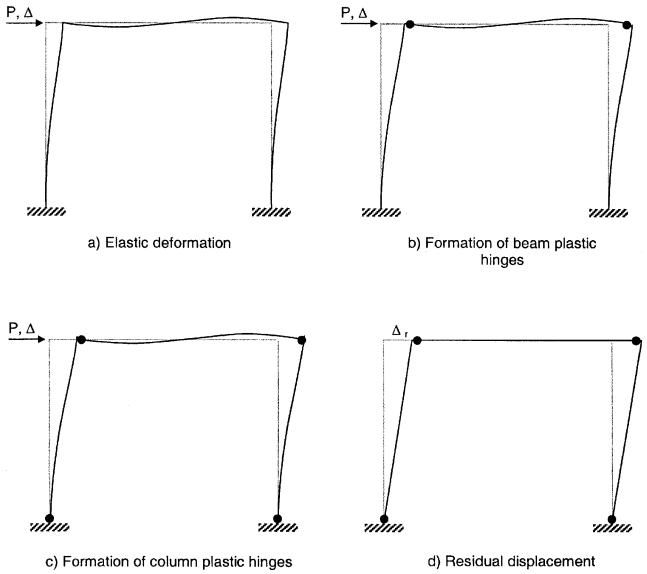

Fig. 3—Deformation sequence of steel-reinforced frame configuration.

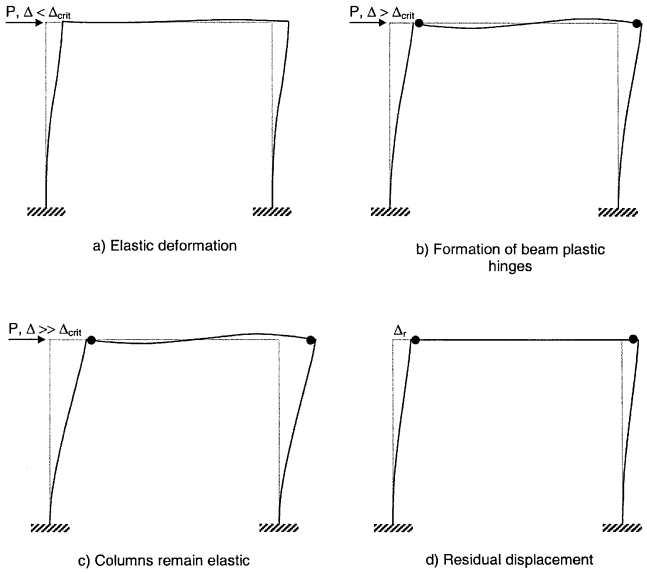

Fig. 5—Deformation sequence of suggested frame configuration.

yielding, a limited flexural load increase may be observed due to internal stress redistribution approaching the member ultimate flexural capacity M_p at deflection Δp enhanced by strain hardening of the steel reinforcement.

Considering a portal frame configuration with steel-reinforced beam and column members, the sequential deformation stages are characterized by elastic behavior (Fig. 3(a)), formation of a first set of plastic hinges in the beam (Fig. 3(b)), followed by a second set of plastic hinges at the column bases (Fig. 3(c)). Further displacement of this statically unstable structure occurs at constant horizontal load, assuming elastic/plastic member deflections (Fig. 2). At unloading, the frame remains in its deflected shape after some elastic retraction at a residual displacement Δr (Fig. 3(d)). Besides the cross-sectional properties of the beam and column members, the geometry of the portal frame, in particular, the ratio of column-to-beam length, may lead to the formation of plastic hinges in the columns prior to hinging in the beam, which, however, results in a kinematic mechanism as well.

In FRP-reinforced members, yielding does not occur and the member deforms linearly to a certain extent and is nearly elastic up to failure (Fischer and Li 2003). At relatively large deflections, successive flexural crack formation along the member and inelastic matrix deformations in compression result in a reduction of flexural stiffness and nonlinearity of the load-deformation response. FRP reinforcement materials generally have a lower elastic modulus compared to steel and, consequently, the flexural stiffness of an FRP-reinforced member at a given reinforcement ratio is lower; however, its flexural strength exceeds that of the steel-reinforced member (Fig. 4). Thus, by selecting an appropriate type and amount of FRP reinforcement, structural members with a given geometry can be designed for flexural strength independent of flexural stiffness, that is, higher strength does not necessarily imply higher stiffness as in the case of exclusive use of mild steel reinforcement.

In a portal frame assembled from a steel-reinforced beam and FRP-reinforced columns, the load-deformation response can be schematically described with an idealized graph of the isolated beam and column flexural response characteristics (Fig. 4) at sequential frame deformation stages (Fig. 5). At frame displacements below Δ_{crit} prior to the formation of plastic hinges, the beam has a larger stiffness than the columns and therefore experiences relatively small, elastic deflections, while the relatively soft, elastic columns largely accommodate the imposed frame displacement in a double curvature deflection mode (Fig. 5(a)). At this deformation stage, the frame responds at an initial, relatively large stiffness and damage

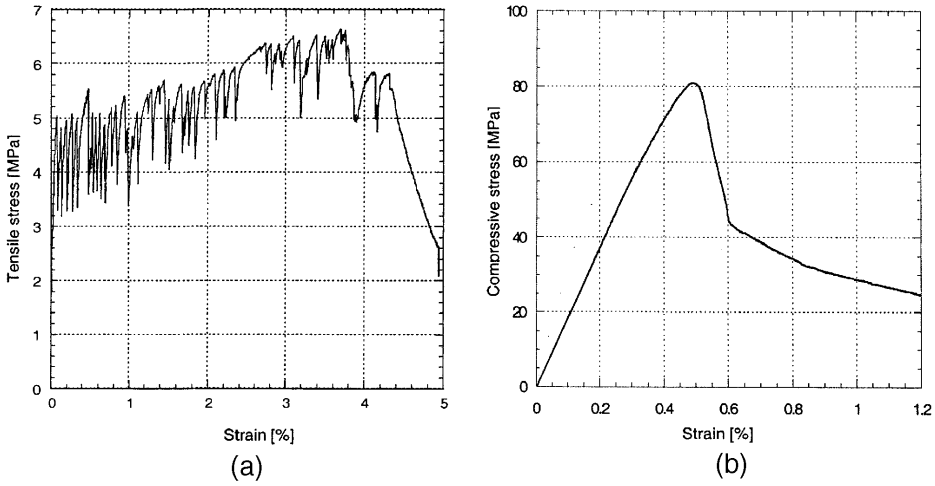

Fig. 6—Stress-strain behavior of ECC in: (a) tension; and (b) compression.

Table 1—Summary of material properties

Reinforcement material	Diameter, mm	E*	f_y†	ε_y‡	f_u§	ε_u‖
Steel	10	210	410	0.2	600	15
Aramid#	8	54	—	—	1800	3.8
CFRP (CFCC)#	6.2 (effective)	137	—	—	1800	1.8
CFRP (LL reinforcement)#	8	147	—	—	1800	1.3

*Elastic modulus, GPa.
†Tensile strength at yield, MPa.
‡Tensile strain at yield, %.
§Tensile strain at ultimate, MPa.
‖Tensile strain at ultimate, %.
#Specified properties.

occurs mainly by crack formation in the column elements and the frame resumes its undeformed shape after unloading.

If displaced beyond Δ_{crit}, the frame modifies its deformation mode and adapts to the increased level of loading by converting into a strong, stiff column/weak, soft beam mechanism (Fig. 5(b)), effectively responding at a lower, secondary frame stiffness. Due to the flexural strength differential between beam and columns, plastic hinges are formed in the beam and energy is dissipated by inelastic deformation of the steel reinforcement. During this deformation stage, the columns remain elastic (Fig. 5(c)) and provide resistance against collapse of the structure, that is, require increasing load to increase frame displacements. After unloading, permanent displacement of the frame Δ_r is due to residual rotation at the beam-column joint imposed by inelastic deformation in the plastic hinge of the beam (Fig. 5(d)).

The details of the response—that is, initial and secondary stiffness—as well as transition displacement Δ_{crit} and transition load P_{crit}, can be adjusted to structural performance requirements defined by the level of acceptable temporary and permanent displacements at expected levels of excitation. Besides reduced residual displacements and the absence of a potential collapse mechanism, this frame configuration provides auto-adaptive response control by adjusting its system stiffness depending on the level of lateral excitation, effectively increasing the period of the structure and consequently decreasing base shear forces experienced during a seismic event.

Material composition and properties

In this study, several types of FRP, as well as steel, were used as longitudinal reinforcement in the columns of the frame specimens, while the beams were generally reinforced with steel reinforcing bars.

Specifically, the selection of FRP reinforcement included CFCC (carbon FRP, stranded tendon), LL (carbon FRP, solid rod), and TR (aramid FRP). Material properties of the FRP reinforcement reported as follows are specified values provided by the manufacturer.

CFCC is a stranded tendon (effective ∅6.2 mm) with 1800 MPa tensile strength, elastic modulus of 137 GPa, and elastic strain capacity of 1.8%. LL reinforcement is a solid rod (∅8 mm) with indented surface geometry and specified tensile strength of 1800 MPa, an elastic modulus of 147 GPa, and a tensile strain capacity of 1.3%. TR reinforcement (∅8 mm), with a surface geometry similar to that of conventional steel reinforcement, has a tensile strength of 1800 MPa, an elastic modulus of 54 GPa, and a tensile strain capacity of 3.8%. In compression, explicit data for the FRP reinforcement are not available; however, the compressive strength and strain capacity are assumed to be approximately 10% of the respective values in tension, as suggested in design guidelines (Sonobe, Fukuyama, and Okamoto 1995).

Mild steel reinforcement used for longitudinal reinforcement has a ribbed surface geometry, a yield strength of 410 MPa, an elastic modulus of 210 GPa, a yield strain of approximately 0.2%, and an ultimate strength of approximately 600 MPa at 15% strain. Diagonal steel reinforcement (∅4 mm) used at the joint region has a smooth surface and a yield strength of 315 MPa at 0.2% strain. The properties of the longitudinal reinforcement materials used in this investigation are summarized in Table 1.

The ECC matrix used 1.5%-volume polyethylene fibers, cement, fine aggregates (maximum grain size 0.25 mm), water, high-range water-reducing admixture, and admixtures to enhance the fresh properties of the mixture. Material properties in uniaxial tension obtained from tensile plate tests of this composition were first cracking strength of 4.5 MPa at 0.01% strain and ultimate tensile strength of 6.5 MPa at approximately 3.8% strain (Fig. 6(a)). The compressive strength of this particular version of ECC was obtained from cylinder tests and was found to be 80 MPa at a strain of 0.5% (Fig. 6(b)). The elastic modulus of this particular version of

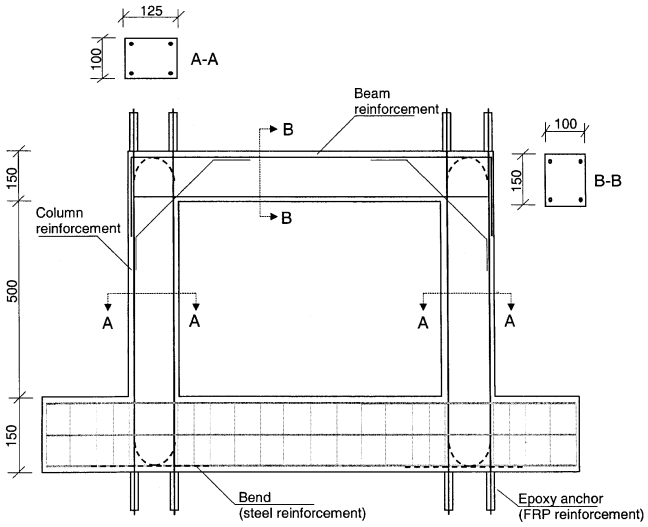

Fig. 7—Specimen configuration.

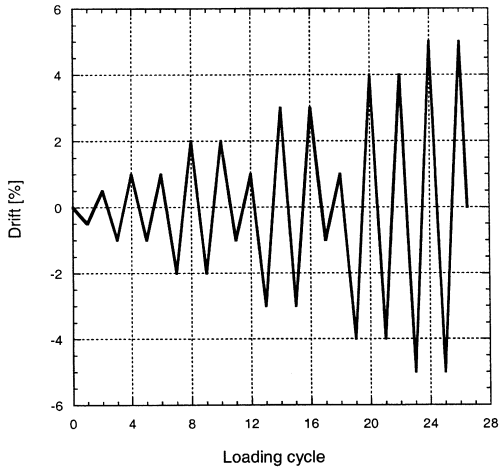

Fig. 8—Loading sequence.

ECC was 18 GPa and was considerably lower than that of typical concrete due to the lack of large aggregates in ECC.

EXPERIMENTAL PROGRAM

Specimen and loading configuration

The response mechanism previously outlined was investigated using a portal frame specimen configuration with a column height of 635 mm and a beam length of 660 mm. Cross-sectional dimensions of the beam were 150 x 100 mm, and columns were 125 x 100 mm. In order to provide fixed-end conditions at the column bases, a rigid base beam was integrally cast with the specimen (Fig. 7). In those specimens with FRP-reinforced columns, the longitudinal FRP bars were extended through the base and externally anchored, whereas in the specimen with steel-reinforced columns, the steel reinforcing bars were bent at a 90-degree angle at the bottom of the base and further extended to provide sufficient anchorage. Lateral loading was applied through a loading frame equipped with a 100 kN-capacity actuator according to a displacement-controlled loading sequence (Fig. 8). A steel pin was mounted at midspan of the beam member to introduce the lateral load while the base was fixed to the loading frame (Fig. 9). Axial load was not applied to the column members.

The specimens were instrumented with a displacement transducer at the top of the frame to measure the total deflection

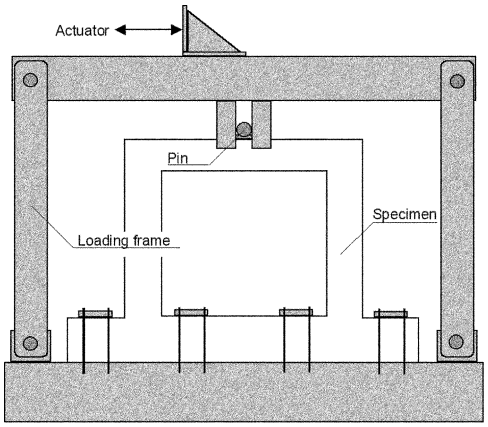

Fig. 9—Experimental test setup.

Table 2—Summary of specimen configurations

	Columns				Beam (steel reinforced)		
	Reinforcement	EI_{cr}*	M_y†	M_p‡	EI_{cr}*	M_y†	M_p‡
S-1	Steel	19.1	6.0	8.0	21.3	5.0	7.5
S-2	Aramid	4.2	—	12.5	13.3	2.9	3.5
S-3	CFRP (CFCC)	6.5	—	14.5	13.3	2.9	3.5
S-4	CFRP (LL)	9.9	—	17.4	21.3	5.0	7.5

*Flexural stiffness of cracked section * 10^{10}, Nmm^2.
†Moment capacity at yielding of longitudinal reinforcement, kNm.
‡Moment capacity at ultimate, kNm.

of the specimens, while the applied lateral load was monitored from the load cell of the actuator. Due to the relatively small diameter of the beam reinforcement in particular, detailed strain gage readings were not obtained from the longitudinal reinforcement of the beam and columns.

In this paper, results from tests on four frame specimens are presented. The beam and column members of all specimens were provided with two pairs of reinforcing bars having a clear cover of 15 mm (Fig. 7). To maintain sufficient beam/column interaction, two diagonal steel rods (∅4 mm) were placed at each joint to assure flexural deformations and prevent beam sliding. Transverse reinforcement in the form of stirrups was not used in the frame specimens except in the base.

More specifically, Specimen S-1 had steel-reinforced columns (reinforcing bar ∅10 mm) and a steel-reinforced beam (reinforcing bar ∅8 mm), Specimen S-2 had aramid-FRP-reinforced columns (reinforcing bar ∅8 mm) and a steel-reinforced beam (reinforcing beam ∅6 mm), Specimen S-3 had CFRP-reinforced columns (effective reinforcing bar ∅6.2 mm) and a steel-reinforced beam (reinforcing bar ∅6 mm), and Specimen S-4 had CFRP-reinforced columns (reinforcing bar ∅8 mm) and a steel-reinforced beam (reinforcing bar ∅8 mm). Due to the lower flexural stiffness of the columns in Specimens S-2 and S-3 compared with Specimens S-1 and S-4, the beam in S-2 and S-3 was designed for lower yield strength to initiate yielding at relatively small frame displacements similar to those in S-1 and S-4.

Details of the specimen configurations including individual member flexural stiffness and expected strength are summarized in Table 2.

EXPERIMENTAL OBSERVATIONS

In all specimens, the crack formation was marked at each consecutive target drift level. Damage was generally limited to the initiation and propagation of flexural and shear cracking

(Fig. 10). Further damage by matrix spalling, compression failure, shear failure, or reinforcement rupture was not observed prior to termination of testing at 5% drift.

In Specimen S-1 (steel-reinforced columns, steel-reinforced beam), flexural cracking initiated at 0.5% drift (15 kN) at the beam ends as well as column bases and, to a limited extent, at the top of the columns. At further increasing deformation, a deviation from elastic behavior becomes apparent in the load-deformation response beyond 1% drift (40 kN) (Fig. 11(a)), when the number of flexural cracks increased significantly in the beam, while further cracking at the column bases was initiated due to shear stresses as indicated by their inclination. Beyond 2% drift (60 kN), the load-deformation curve reached a plateau, while the number of cracks at the top of the columns stabilized and additional crack formation was concentrated at the beam ends as well as column bases. Flexural cracking extended approximately one member depth above the column base and two member depths from the beam/column interface. At 4% drift (65 kN), cracking localized at the beam-column interface and further increasing frame displacement was accompanied by increasing crack width at this location (Fig. 10(a)).

In Specimen S-2 (aramid-FRP-reinforced columns, steel-reinforced beam), crack formation initially occurred predominantly in the column members (top and base) at deflections up to 1% drift (25 kN) (Fig. 11(b)). The extent of flexural cracking at the top of the column was similar to that at the column base, while the beam was nearly uncracked. At 2% drift (40 kN), the number of flexural cracks at the beam ends increased significantly together with that at the column bases, while crack formation stabilized at the top of the column. At 3% drift (50 kN), further flexural cracking was largely limited to the beam ends and column bases and continuously initiated at these locations at 4% drift (60 kN) (Fig. 10(b)) and 5% drift (65 kN).

Similar to Specimen S-2, initial crack formation in Specimen S-3 (CFRP reinforced columns, steel-reinforced beam) occurred primarily in the column members (top and base). Major flexural cracking in the beam was observed beyond 1% drift (35 kN) (Fig. 11(c)), accompanied by further flexural cracking in the columns extending from the bases over a considerable portion of the column members. At loading cycles up to 2% drift (45 kN), the column members showed a well-distributed flexural crack pattern throughout their entire height. Beyond 3% drift (53 kN), additional deformation demand at the column bases was accommodated by the formation of shear cracking. Flexural crack formation continued in the beam up to 4% drift (60 kN) and extended approximately two member depths from the beam-column interface (Fig. 10(c)).

In Specimen S-4 (CFRP reinforced columns, steel-reinforced beam), flexural cracking occurred in the beam element at 1% drift (30 kN), while the deformation of the column members was almost immediately dominated by shear cracking. At 2% drift (60 kN), the columns showed evenly distributed shear crack formation throughout their entire height with a limited number of flexural cracks at the column bases. At increasing drift levels, the applied lateral load remained constant resulting in apparently ductile load-deformation response, while the number of shear cracks in the column increased continuously with further flexural crack formation in the beam. At this stage, the applied lateral load in the second loading cycle at given target displacement was significantly smaller compared to the initial loading cycle (Fig. 11(d)).

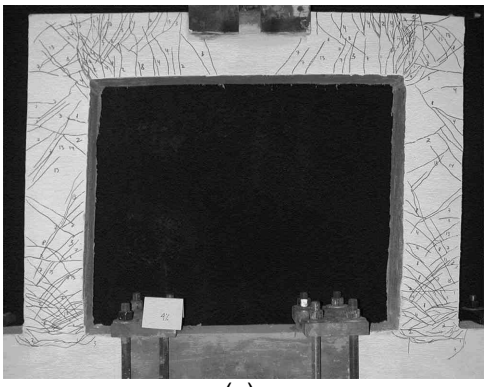

(a)

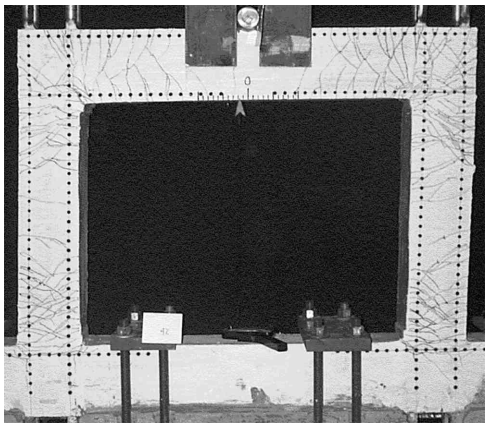

(b)

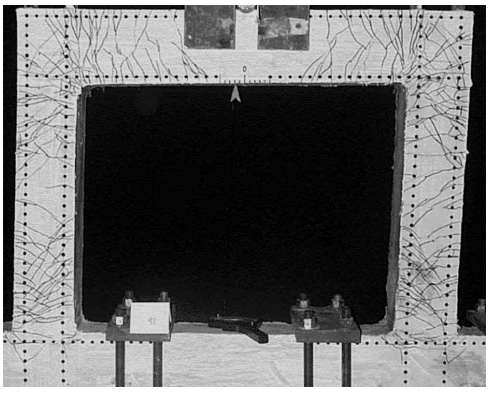

(c)

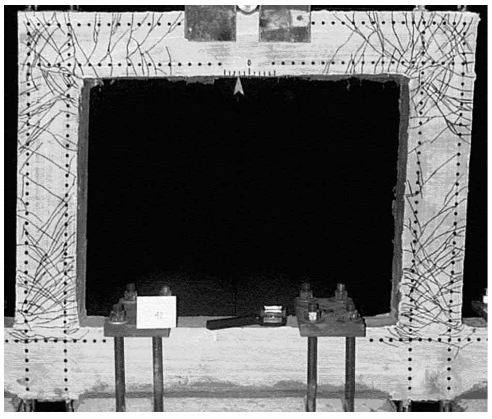

(d)

Fig. 10—Deformed shape at 4% drift of: (a) Specimen S-1; (b) Specimen S-2; (c) Specimen S-3; and (d) Specimen S-4.

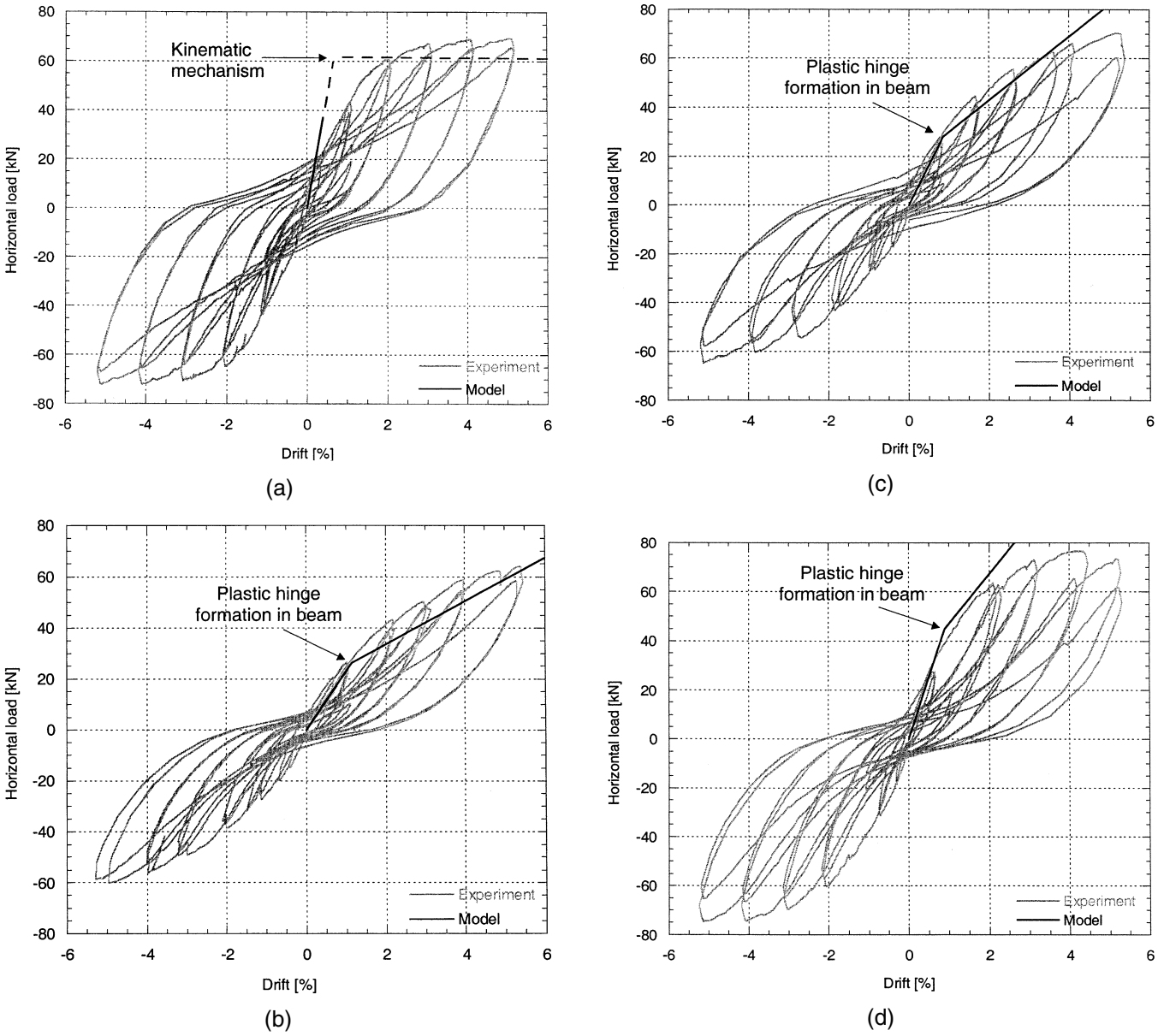

Fig. 11—Load deformation behavior of: (a) Specimen S-1 (steel-reinforced columns, steel-reinforced beam); (b) Specimen S-2 (aramid-reinforced columns, steel-reinforced beam); (c) Specimen S-3 (CFRP-reinforced columns, steel-reinforced beam); (d) Specimen S-4 (CFRP-reinforced columns, steel-reinforced beam).

Beyond 4% drift (75 kN), minor crushing of the ECC matrix was observed (Fig. 10(d)).

DISCUSSION

The response mechanism of the suggested frame configuration (S-2, S-3, and S-4) is contrasted with the control specimen (S-1) and analyzed from a qualitative and conceptual rather than strictly quantitative viewpoint. The evaluation of the specimens particularly focuses on the change in response at yielding of the beam member, as indicated by increased formation of cracking at the beam ends, as well as based on theoretical considerations taking into account the flexural strength and stiffness of the beam and column members. Furthermore, the comparison of Specimens S-2, S-3, and S-4 is used to obtain an understanding of the potential to control and modify the structural response and explore possible failure modes of the suggested configuration.

Load-deformation response

The load-deformation diagram and experimental observations of Specimen S-1 (Fig. 11(a)) indicate an elastic/plastic response due to the combination of steel-reinforced beam and columns. Preliminary calculations indicated that yielding of the beam coincides with yielding of the column at an applied load of 38 kN. The onset of inelastic frame deformation becomes apparent in the experimentally obtained load-deformation graph at approximately 1% drift (40 kN) due to initiation of yielding in the longitudinal steel reinforcement of the columns. A significant reduction in flexural stiffness occurs at 2% drift (60 kN) as a result of the formation of plastic hinges in the columns and the beam. Inelastic deformations are accompanied by an increasing number of flexural cracks at the plastic hinge locations at the beam ends and column bases. Beyond full plasticity of the beam and column members, only a slight increase in applied load can be observed up to 5% drift (68 kN). Despite very stable inelastic

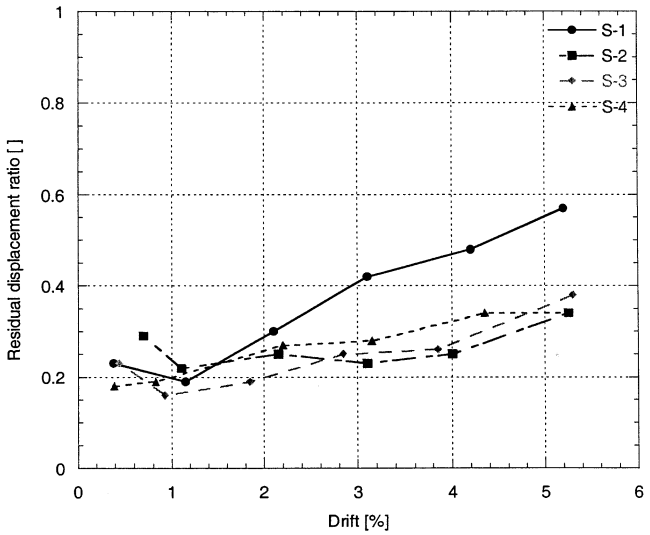

Fig. 12—Residual displacement ratio after unloading from target drift level.

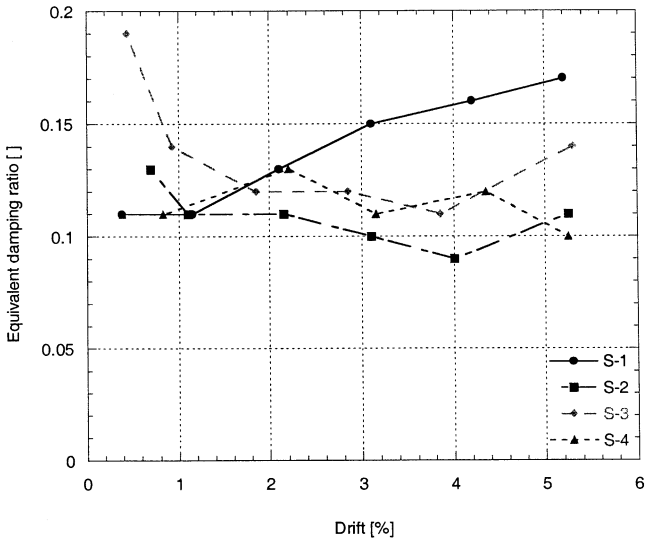

Fig. 13—Equivalent damping ratio.

deformation of the frame beyond 2% drift, the structure has formed a complete kinematic mechanism due to the formation of four plastic hinges in the beam and column members.

Specimen S-2 (Fig. 11(b)) shows a significantly lower initial stiffness compared to Specimen S-1, primarily due to a lower flexural stiffness of the FRP-reinforced columns, but also because of a lower strength and stiffness of the steel reinforced beam. The reduction in reinforcement ratio in the beam member of Specimen S-2 was necessary to initiate beam yielding at relatively small frame deformations at given FRP reinforcement ratio in the columns. The predominant formation of flexural cracking at the top and base of the columns suggests that frame deformations below 1% drift (25 kN) are primarily accommodated by double curvature column deflections, while the beam remains elastic. Beyond 1% drift, the yield strength of the beam member is reached and the formation of plastic hinges results in inelastic rotations at these locations and the columns accommodating further frame deformations as cantilevers with a plastic moment ($M_{p,\,\mathrm{beam}}$) applied at the beam/column joint. This transition leads to a change in frame stiffness with continuing elastic column deformations, which require increasing load to further increase frame displacements, that is, provide non-zero stiffness. Permanent rotation in the beam plastic hinges, however, causes some residual frame deformation at unloading (Fig. 11(b)). The frame continues to deform in this mode up to 5% drift (60 kN) without failure.

In Specimen S-3 (Fig. 11(c)), the transition between initial and secondary response mode is more pronounced than in Specimen S-2 due to a considerably larger flexural stiffness of the CFRP-reinforced columns (Table 2). At yielding of the beam member at 2% drift (45 kN), the change in frame stiffness becomes apparent in the load-deformation graph. Prior to this stage, the column members deform in a double-curvature mode and cracking occurs primarily in the columns. Similar to Specimen S-2, beyond formation of plastic hinges in the beam, the secondary stiffness of the frame is due to the cantilever deflection of both columns with the beam plastic moment ($M_{p,\,\mathrm{beam}}$) applied at the beam/column joint. At further increasing frame deformations, shear cracking in the column members indicates that the applied frame shear force exceeded the cracking strength of ECC, however, could not surpass the ultimate shear capacity of the member.

Specimen S-4 (Fig. 11(d)) shows an initial stiffness similar to that of Specimen S-1 and considerably larger than that of Specimens S-2 and S-3. Starting at relatively small deflections, the continuing formation of shear cracking dominates the formation of flexural cracking, suggesting a flexural stiffness of the columns in excess of the shear stiffness. A change in frame stiffness becomes apparent beyond 2% drift (60 kN) followed by virtually plastic deformation at 4% drift (75 kN). This significant reduction in frame stiffness is caused by yielding of the beam as well as continuing formation of shear cracking in the columns, which results in apparently ductile load-deformation behavior of the frame. Due to these inelastic shear deformations, the repeat loading cycles at 4 and 5% drift in Specimen S-4 show a significantly lower applied load compared with the initial loading cycle.

Residual displacement and energy dissipation

The residual displacement ratio is considered herein as the residual displacement at unloading normalized by the target displacement at each drift level. Energy dissipation is expressed in terms of the equivalent damping ratio that characterizes the shape of the hysteresis loops by relating the energy dissipated in one complete deformation cycle to the maximum strain energy at a given displacement amplitude (Chopra 1995).

The mechanisms contributing to the residual displacement and energy dissipation include the formation of cracking in ECC, the formation of plastic hinges in the beam (and columns in Specimen S-1), as well as permanent rotation in the beam plastic hinges resulting in permanent deflection of the columns and consequently of the frame (Fig. 5(d)). Therefore, despite the elastic deformation behavior of the FRP-reinforced columns, the residual displacement of the suggested frame configuration can only be reduced to a certain extent due to permanent frame deformations induced by the inelastic deformation behavior of the steel reinforced beam.

In Specimen S-1, the residual displacement ratio (Fig. 12) is relatively small at lower drift levels however gradually increases at further increasing drift due to the formation of plastic hinges in the beam and column members. After experiencing 5% drift, the residual displacement ratio is approximately 0.57. Similarly, the equivalent damping ratio (Fig. 13) is initially small and gradually increases beyond

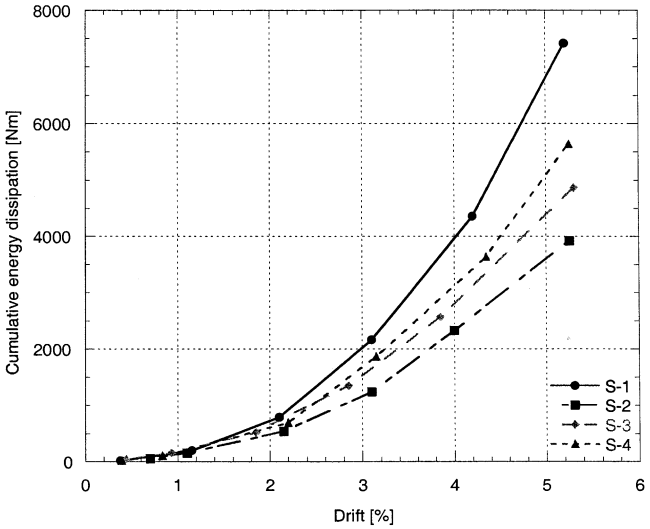

Fig. 14—Cumulative energy dissipation.

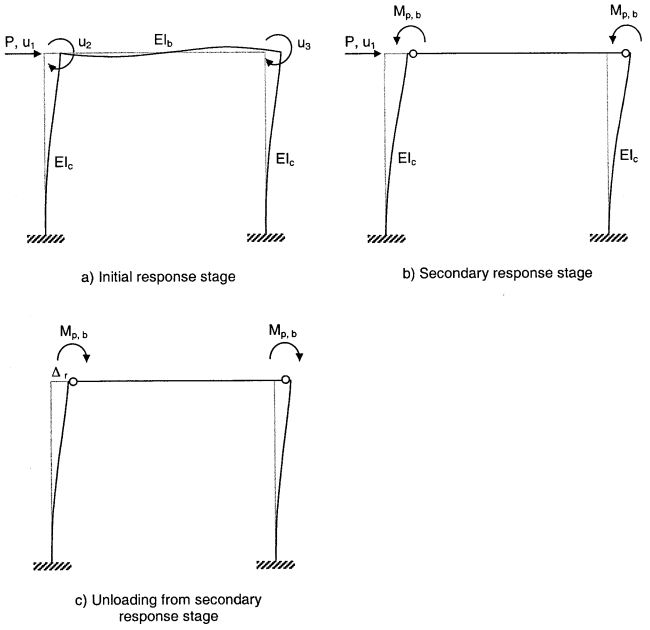

Fig. 15—Modeling of initial and secondary response.

formation of plastic hinges due to energy dissipation by inelastic frame deformations.

In contrast, the residual displacement ratio in Specimen S-2 is initially larger than that of Specimen S-1, due to the more significant effect of matrix crack formation at lower flexural resistance, however, remains nearly constant at approximately 0.25 at increasing frame displacements up to 4% drift. After experiencing 5% drift, the residual displacement ratio in Specimen S-2 is approximately 0.35.

Similar trends can be observed in the development of the equivalent damping ratio, however, with a slight decrease in damping up to 4% drift. In all specimens, continuing crack formation in the ECC matrix at increasing flexural displacements causes a difference between the initial and reloading flexural stiffness, which for practical purposes is insignificant in absolute terms. Besides the contribution of crack formation to energy absorption in Specimen S-2, only the beam is undergoing inelastic deformations and, consequently, less energy is dissipated in Specimen S-2 as compared with Specimen S-1 where the formation of plastic hinges at the column bases contributes significantly to the total energy dissipation capacity (Fig. 14). The direct comparison indicates a cumulative energy dissipation (initial and reloading cycles) in Specimen S-2 of approximately half of that in Specimen S-1, which is conceivable considering the contribution of plastic hinges in the columns in S-1. In a multi-story frame structure, however, the absent contribution of inelastic deformation at the column base of the suggested frame configuration is expected to be relatively small compared with that dissipated in the beam plastic hinges of the entire structure.

Due to the influence of shear cracking in Specimens S-3 and S-4, the residual displacement ratio increases slightly at increasing deformations (Fig. 12) while the equivalent damping ratio also increases slightly at large drift levels (Fig. 13), suggesting that inelastic shear deformations in the ECC matrix could be a potential source of energy dissipation as well as a gradual failure mode of the column members. This is also indicated in the cumulative energy dissipation of Specimen S-3 and S-4 compared to Specimen S-2 (Fig. 14).

Modeling of load-deformation envelope

The analysis of the load-deformation response of the suggested frame configuration presented in this paper will focus on capturing the intended bilinear load-deformation mechanism in a simplified approach based on the flexural behavior of the beam and column members. At this stage, it is not intended to incorporate further details of the frame deformation mechanism, such as joint distortions and shear deformations, which are not unique to the suggested frame configuration.

The response of the portal frame structure discussed in this paper can be separated into a model for the initial stage prior to yielding of the beam and the secondary stage beyond yielding of the beam, assuming elastic behavior of the columns during both stages. The response in the initial stage when beam and columns are both deforming elastically can be modeled using the static condensation method (Chopra 1995), taking into account the flexural stiffness and strength of the frame members (Fig. 15(a)). Beyond the formation of plastic hinges in the beam, the frame system can be considered consisting of two cantilever beams with a moment equal to the plastic moment of the beam applied at beam/column joint (Fig. 15(b)).

During the initial deformation stage, the flexural stiffness EI_{cr} of the frame members is derived assuming cracked member sections and a fixed position of the neutral axis. These assumptions greatly simplify the approach but are expected to underestimate frame displacements at larger drift levels since nonlinear deformations in the cementitious matrix under compression are not incorporated. At the transition from the initial to the secondary response stage, however, these nonlinear deformations in ECC are expected to be insignificant.

The frame response during the initial deformation stage can be generally expressed as

$$\underline{P} = \underline{\underline{K}}\,\underline{u}$$

where $\underline{P}$ is the vector of applied loads, $\underline{\underline{K}}$ is the system stiffness matrix, and $\underline{u}$ is the deformation vector. For the portal frame structure used in this study, the degrees of freedom are the horizontal displacement u_1 at the load point and the joint rotations u_2 and u_3 (Fig. 15(a)). Considering the stiffness

and geometry of the beam and column members, the lateral applied load P is related to the horizontal displacement u_1 as

$$P = Ku_1$$

with K being determined by solving the matrix equations. Using the lateral displacement u_1 and the joint rotations u_2 and u_3, the internal moments in the frame members can be derived as a function of the horizontal frame displacement u_1 (Fischer 2002).

From this procedure, the initial response stage of the tested specimens is determined with varying degree of accuracy. For Specimen S-1, the experimentally obtained stiffness is significantly overestimated in the model (Fig. 11(a)), which may be partly influenced by shear deformations occurring at early stages of loading. According to the model, the onset of inelastic deformation in Specimen S-1 occurs at an applied load of 38 kN when yielding in the beam and columns effectively coincide at a displacement of 0.55% drift, which compares to an actual frame displacement of approximately 1% drift at the onset of inelastic deformation.

The ultimate capacity of Specimen S-1 is determined from plastic analysis as 62 kN, based on the ultimate moment capacity M_p of the beam and column members, assuming yielding and strain hardening of the longitudinal steel reinforcement. Considering the experimentally obtained load-deformation response of Specimen S-1, the ultimate capacity (68 kN) slightly exceeds the theoretical value. Beyond onset of yielding in beam and columns, the modeled frame response was extended elastically up to reaching the ultimate loading capacity of the frame (62 kN).

In Specimens S-2, S-3, and S-4 (Fig. 11(b) through 11(d)), the prediction of the initial response generally agrees with the experimental data however slightly underestimates the initial stiffness. The contribution of the ECC matrix to the flexural resistance has been neglected in the analysis because its load-carrying contribution relies on an unrepeatable fiber pullout mechanism. After this mechanism has been utilized in the first loading cycle at each drift level, the tensile component in the cross section of the column member is largely determined by the longitudinal reinforcement and, therefore, the load-deformation path in the second loading cycle at each drift level differs from the first by the flexural strength contribution of ECC in tension. This nonrecurring contribution is particularly significant in members with low reinforcement ratio and/or low modulus longitudinal reinforcement.

Beyond formation of plastic hinges in the beam of Specimens S-2, S-3, and S-4, the frame is modeled as two cantilever columns with an applied moment $M_{p,b}$, resulting in

$$u_1 = \frac{1}{EI_g}\left[\frac{P}{12}(L-l_{cr})^3 + \frac{1}{2}\left(M_{p,b} - \frac{P(L-l_{cr})}{2}\right)(L-l_{cr})^2\right]$$

$$+ \frac{1}{EI_{cr}}\left[\frac{P}{4}l_{cr}^2 + \left(M_{p,b} - \frac{PL}{2}\right)l_{cr}\right](L-l_{cr}) + \frac{1}{EI_{cr}}$$

$$\left[\frac{P}{12}(L-l_{cr})^3 + \frac{1}{2}\left(M_{p,b} - \frac{PL}{2}\right)(L-l_{cr})^2\right]$$

with the cracked length of the columns

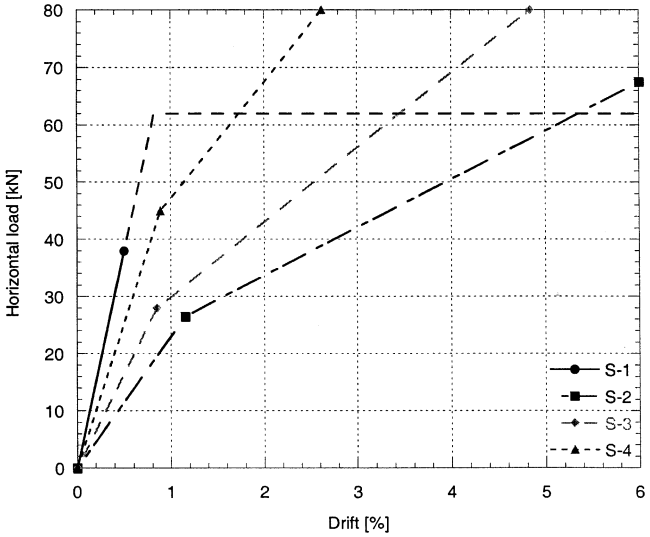

Fig. 16—Model response of tested specimens.

$$l_{cr} = \left(\frac{4\sigma_{cr}I_g}{Ph} + L - \frac{2M_{p,b}}{P}\right)$$

Similar expressions were derived and elaborated on for FRP-reinforced flexural members under cantilever-type loading conditions (Fischer and Li 2003). Using the member properties of Specimens S-2, S-3, and S-4 in terms of geometry, flexural stiffness, and strength (Table 2) in the aforementioned expressions, the resulting theoretical response visualizes the intended two-stage response mechanism of the suggested configuration with an initial system stiffness prior to yielding in the beam and a subsequent secondary stiffness due to cantilever deformation of the columns (Fig. 16). The range of initial and secondary response obtained from these particular configurations indicates the potential to design for a specific system behavior by using suitable combinations of beam and column stiffness and strength, that is, reinforcement type and ratio. The comparison with the model of a conventional steel-reinforced configuration further indicates the basic difference of the bilinear response of the suggested system as opposed to an elastic/plastic response and ultimate kinematic mechanism (S-1). The theoretically derived load-deformation relationship closely predicts the transition point between initial and secondary response stage, as well as the secondary stiffness in Specimen S-2 (Fig. 11(b)). Analogous to the initial response, the contribution of the ECC matrix in the first loading cycle at each drift level should be disregarded to evaluate the accuracy of the model. In Specimen S-3, model and experimental data agree up to 4% drift, beyond which shear deformations softened the load-deformation response of the specimen (Fig. 11(c)). This softening mechanism is unaccounted for in the current model. The influence of these shear deformations is significantly more pronounced in Specimen S-4, and, subsequently, the model and experimental data deviate considerably beyond 2% drift (Fig. 11(d)).

CONCLUSIONS

The intended deformation mechanism of the frame configuration introduced in this study has been experimentally verified and theoretically modeled. The interaction of structural composite elements with elastic and elastic/plastic load-deformation behavior results in a bilinear frame response characterized by an initial and secondary

stiffness, reduced residual displacements, and energy dissipation capacity. In contrast to conventional moment-resisting frames assembled exclusively from steel-reinforced members, in the suggested frame configuration, the formation of plastic hinges in the steel-reinforced beam is initiated and used for energy dissipation without formation of plastic hinges at the column bases and consequently does not result in a potential collapse mechanism. The transition between initial and secondary response is inherent in the structure and can be designed to meet specific performance requirements.

The experimentally obtained response of the suggested frame configuration can be adequately modeled assuming elastic/plastic load-deformation behavior of the beam and elastic behavior of the column elements. The relatively large elastic deflection capacity of these composite columns is achieved in this particular case by combining elastic FRP reinforcement with a ductile ECC. Due to the damage-tolerant deformation behavior of ECC, structural damage is limited to controlled inelastic deformations by crack formation in ECC and yielding of beam reinforcement.

Besides the immediate benefits of a collapse-resistant frame structure with reduced residual deflections and rehabilitation requirements, presented herein without axial loading and at small lateral displacements, the effect of auto-adaptive stiffness modification at transition from initial to secondary frame stiffness is expected to increase the period of the structure and consequently reduce the base shear forces in this structural system in case of seismic excitation.

Future research activities will be directed to the effect of axial loading, especially on the compressive strain demand in the FRP reinforcement and subsequent limitations of the column deflection capacity, as well as substituting FRP reinforcement in the column members with high-strength steel tendons with a relatively large elastic tensile strain capacity exceeding that of conventional mild steel reinforcement.

ACKNOWLEDGMENTS

The research activities described in this paper have been supported by a grant from the National Science Foundation (CMS-0070035) to the ACE-MRL at the University of Michigan. This support is gratefully acknowledged.

NOTATION

E = modulus of elasticity of cementitious matrix
h = height of column cross-section
I_{cr} = moment of inertia (cracked)
I_g = moment of inertia (uncracked)
L = length of column
l_{cr} = length of cracked section
$M_{p,b}$ = moment capacity of beam at ultimate
P = horizontal load
u_1 = horizontal frame displacement
u_2, u_3 = beam/column joint rotation
σ_{cr} = tensile strength of cementitious matrix

REFERENCES

ACI Committee 440, 1996, "State-of-the-Art Report on Fiber Reinforced Plastic (FRP) Reinforcement for Concrete Structures (440R-96)," American Concrete Institute, Farmington Hills, Mich., 65 pp.

Alsayed, S. H., and Alhozaimy, A. M., 1999, "Ductility of Concrete Beams Reinforced with FRP Bars and Steel Fibers," *Journal of Composite Materials*, V. 33, No. 19, pp. 1792-1806.

Chopra, A. K., 1995, *Dynamics of Structures—Theory and Applications to Earthquake Engineering*, Prentice-Hall, Inc., pp. 94-100.

El-Sheikh, M. T.; Sause, R.; Pessiki, S., 1999, "Seismic Behavior and Design of Unbonded Post-Tensioned Precast Concrete Frames," *PCI Journal*, May-June, pp. 54-71.

Fischer, G., 2002, "Deformation Behavior of Reinforced ECC Flexural Members under Reversed Cyclic Loading Conditions," PhD dissertation, University of Michigan, Ann Arbor, Mich.

Fischer, G., and Li, V. C., 2002, "Effect of Matrix Ductility on Deformation Behavior of Steel Reinforced ECC Flexural Members under Reversed Cyclic Loading Conditions," *ACI Structural Journal*, V. 99, No. 6, Nov.-Dec., pp. 781-790.

Fischer, G., and Li, V. C., 2003, "Deformation Behavior of FRP Reinforced ECC Flexural Members under Reversed Cyclic Loading Conditions," *ACI Structural Journal*, V. 100, No. 1, Jan.-Feb., pp. 25-35.

Fukuyama, H.; Masuda, Y.; Sonobe, Y.; and Tanigaki, M., 1995, "Structural Performances of Concrete Frame Reinforced with FRP Reinforcement," *Non-Metallic (FRP) Reinforcement for Concrete Structures*, Proceedings of the Second International RILEM Symposium (FRPRCS-2), E&FN Spon, London, pp. 275-286.

Harris, H. G.; Samboonsong, W.; and Ko, F. K., 1998, "New Ductile FRP Reinforcing Bar for Concrete Structures," *ASCE Journal for Composites for Construction*, V. 2, No. 1, Feb., pp. 28-37.

Kurama, Y.; Pessiki, S.; and Sause, R., 1999, "Seismic Behavior and Design of Unbonded Post-Tensioned Precast Concrete Walls," *PCI Journal*, May-June, pp. 72-89.

Li, V. C., 1998, "Engineered Cementitious Composites—Tailored Composites Through Micromechanical Modeling," *Fiber Reinforced Concrete: Present and the Future*, N. Banthia, A. Bentur, A. and A. Mufti, eds., Canadian Society for Civil Engineering, Montreal, Canada, pp. 64-97.

Naaman, A. E., and Jeong, S. M., 1995, "Structural Ductility of Concrete Beams Prestressed with FRP Tendons," *Non-Metallic (FRP) Reinforcement for Concrete Structures*, Proceedings of the Second International RILEM Symposium (FRPRCS-2), E&FN Spon, London.

Paulay, T., and Priestley, M. J. N., 1992, *Seismic Design of Reinforced Concrete and Masonry Buildings*, John Wiley & Sons, Inc., pp. 98-106.

Priestley, M. J. N.; Sritharan, S. S.; and Conley, J. R., 1999, "Preliminary Results and Conclusions from PRESSS Five-Story Precast Concrete Test Building," *PCI Journal*, Nov.-Dec., pp. 42-67.

Ricles, J. M.; Sause, R.; and Garlock, M. M., 2001, "Post-Tensioned Seismic Resistant Connections for Steel Frames," *ASCE Journal of Structural Engineering*, V. 127, No. 2, Feb., pp. 113-121.

Sonobe, Y.; Fukuyama, H.; and Okamoto, T., 1997, "Design Guidelines of FRP Reinforced Concrete Building Structures," *ASCE Journal of Composites for Construction*, V. 1, No. 3, Aug., pp. 90-115.